Engineering Fracture Mechanics 77 (2010) 768–775

Contents lists available at ScienceDirect

Engineering Fracture Mechanics

journal homepage: www.elsevier.com/locate/engfracmech

Resistance to cleavage cracking and subsequent shearing of high-angle grain boundary

Weiyi Lu [a], Jin Chen [a], Srinivas S. Chakravarthula [b], Yu Qiao [a,*]

[a] Department of Structural Engineering, University of California, San Diego, La Jolla, CA 92093-0085, USA
[b] Department of Civil Engineering, University of Akron, Akron, OH 44325, USA

ARTICLE INFO

Article history:
Received 28 January 2009
Received in revised form 30 November 2009
Accepted 21 December 2009
Available online 28 December 2009

Keywords:
Cleavage
Fracture resistance
Grain boundary
Nonuniform

ABSTRACT

In a previous experimental study, it was observed that the break-through process of a cleavage front across a high-angle grain boundary can be highly nonuniform. While the central part of the boundary can be cleaved quite smoothly, the rest parts must be sheared apart. In this paper, the trapping effect of grain boundary shearing is analyzed in considerable detail. Before the shearing is completed, the crack flanks are locally pinned together and a bridging stress must be provided. The bridging stress has a negative contribution to the local stress intensity at the cleavage front segment that penetrates across the grain boundary, and thus the crack growth driving force must be increased. A closed-form equation is derived to relate the overall fracture resistance to the fracture mode through an energy analysis.

Published by Elsevier Ltd.

1. Introduction

Cleavage cracking is one of the most dangerous failure modes of engineering materials [1]. At the tip of a sharp crack, the high degree of stress concentration can cause rapid separation of atomic or molecular planes, resulting in catastrophic failure with only a relatively small amount of energy being dissipated. That is, the material tends to completely fail when the external loading and the strain energy density are still low, especially when the loading rate is high and/or the temperature is low [2].

Usually, the requirements of toughening and strengthening are contradictory to each other [3]. On the one hand, as a material becomes stronger, its plastic deformation mechanisms are suppressed, and therefore the energy dissipation associated with crack propagation is reduced [4]. On the other hand, to be ductile, it must be relatively easy for a material to undergo plastic deformation in crack-tip zone [5]. One way to solve this problem is to make the material heterogeneous. With a strong yet brittle matrix, if dispersed reinforcements can interrupt cleavage crack growth, the fracture toughness can be increased while the strength is not affected. This concept has been widely employed in polymer [6] and ceramic [7] matrix composites, by using continuous fibers, short fibers, and/or particulates. The fibers and particulates are often made of carbons, metals and alloys, glasses, and/or polymers, which are of high toughness and can be strongly bonded [8]. For metallic materials, however, due to the constraints in processing and application conditions, addition of fillers can be difficult or irrelevant. Under this condition, very often grain boundary is the primary heterogeneity that can raise the resistance to cleavage cracking.

In an early experimental study, Gell and Smith [9] observed that grain boundaries offered important resistance to cleavage crack growth, which is in agreement with the assumption of the classic Griffith theory that precracks are often

* Corresponding author.
E-mail address: yqiao@ucsd.edu (Y. Qiao).

0013-7944/$ - see front matter Published by Elsevier Ltd.
doi:10.1016/j.engfracmech.2009.12.009

grain-sized [10]. It also agreed well with the results of the famous brittle-to-ductile transition experiment of Hahn et al. [11]. In a recent experiment on iron–silicon alloy [12,13], the effects of crystallographic misorientation across high-angle grain boundaries were investigated quantitatively. The grain boundary was characterized by three misorientation angles: the tilt angle (φ), the twist angle (θ), and the rotation angle. It was noticed that the rotation angle had little influence on the grain boundary toughness. Between the rest two factors, the effect of the twist angle was more significant. The effects of φ and θ can be collectively described as

$$\frac{G_{GB}}{2\gamma} = \frac{\sin\theta + \cos\theta}{\cos^2\varphi} + C\frac{\sin\theta \cdot \cos\theta}{\cos\varphi} \tag{1}$$

where G_{GB} is the critical energy release rate of the grain boundary, 2γ is the effective surface free energy of cleavage plane, and C is a material constant dependent on the grain boundary strength and the profile of crack front. The fracture resistance of a polycrystalline material to a uniformly propagating cleavage crack can be analyzed based on Eq. (1), by calculating the average contributions of all the possible values of $\{\varphi, \theta\}$ as well as the influence of lateral grain boundaries [14]:

$$G_{PC0} = \alpha \cdot (2\gamma) \tag{2}$$

The randomness of grain orientation leads to a constant factor, $\alpha \approx 3.2$.

One problem that remains unsolved is, when compared with the experimental data of polycrystalline steels [14–16], Eq. (2) underestimates the overall fracture toughness by an order of magnitude. If only the contributions of the separation of crystallographic planes, the secondary cleavage cracking, and the deformation of ligaments are taken into consideration, the critical energy release rate would be only 0.8 kJ/m^2 [12]. The measured fracture resistance of a polycrystalline 1010 steel under cryogenic condition, however, is around 68 kJ/m^2 [14].

In addition to the work of plastic shearing, the large difference between them may be attributed to that the cleavage front propagation across a field of grains is usually quite nonuniform. To derive Eq. (1), it is assumed that when a cleavage front encounters a high-angle grain boundary, it penetrates through the boundary at a large number of break-through points simultaneously. Because the orientations of cleavage planes across the grain boundary are different, secondary cracking must take place in the grain ahead of the boundary to complete the fracture surface separation, resulting in the river markings parallel to the crack advance direction. The break-through points distribute along the boundary regularly. When the critical penetration depth is reached, the persistent grain boundary islands in between the break-through points are separated apart, so that the grain boundary is bypassed by the cleavage front.

In experiments, however, it was noticed that not all the grain boundaries could be described by such a regular failure mode. For instance, when a cleavage crack advanced in a 1010 steel [14], while regular river markings were observed, at a considerable number of grain boundaries (e.g. the grain boundaries indicated by the arrows in Fig. 1) plastic shearing subsequent to partial cleavage cracking was evident. At these boundaries, cleavage front penetration occurred only in the central parts, and therefore the river markings were radial. The rest sections of the boundaries were separated apart through plastic shearing, which demanded more fracture work. Moreover, as the behaviors of the crack front were different in central and side sections, the distribution of local stress intensity must be nonuniform, which could cause a crack trapping effect. In the past, this irregular failure mode of grain boundary did not receive the necessary attention. In a recent work of Qiao [17], the additional work of plastic shearing was taken into account, but the contribution of the crack trapping effect was ignored, which will be analyzed in detail in the current study.

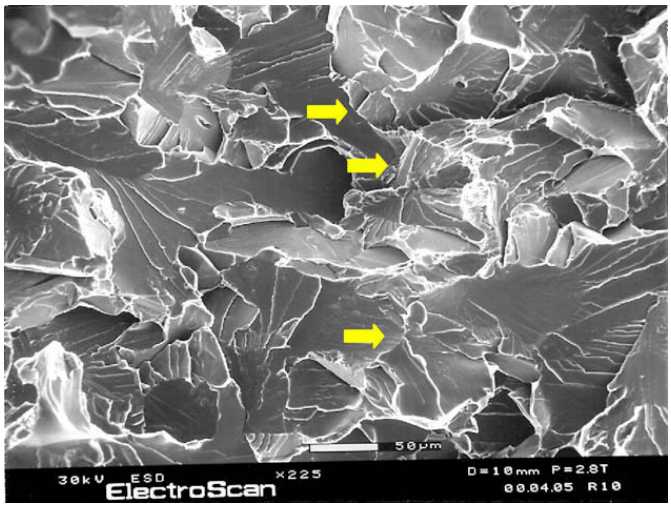

Fig. 1. SEM fractography of cleavage cracking across a field of randomly oriented grains. The crack propagates from the left to the right. The arrows indicate the grain boundaries that are sheared apart after partial cleavage cracking.

2. Trapping effect associated with partial cleavage cracking

Fig. 1 shows SEM fractography of the cleavage cracking process in a 1010 steel at −100 °C. The detailed testing procedure has been discussed elsewhere [14]. Prior to the fracture test, the material had been thermal treated in hydrogen and fully annealed in nitrogen. When the cleavage front bypasses a grain boundary, due to the twist misorientation, river markings are formed. It can be seen that in most of the grains the river markings are parallel to each other, indicating that the front segment is straight when it propagates across the grain. In some grains, e.g. the ones indicated by the arrows, the river markings are radial. They initiate only from the central part of the grain boundary, fanning out into the grains ahead of the boundaries. The boundary sections next to the central part are separated apart via plastic shearing. The cleavage front segments are curved inside these grains, suggesting that the side sections of boundary fail after the central part is broken through.

This process is shown more clearly in Fig. 2, where the crack propagates from the bottom to the top. When the crack front reaches the grain boundary, it is arrested at side sections. In the central part, the front penetrates into the grain ahead of the boundary, leading to the formation of radial river markings. The central part of the boundary, which will be referred to as the break-through window (BTW) in the following discussion, is quite smooth, which minimizes the required fracture work. In the side sections outside the BTW, the direct crack front penetration is not observed. After the front section advances in the next grain in the BTW, as cleavage planes at both sides of the grain boundary are cleaved, the bridging boundary sections are separated through shearing. Since the cleavage facets are planar, the separated boundary sections are triangle shaped.

The mechanism of the irregular grain boundary fracture mode may be related to the chronology of the cleavage front advance. As a crack front propagates across a field of grains, due to the variation in local fracture resistance and the disturbance in external loading, e.g. the grain size distribution, the change in crystallographic orientation, and the mode-II or mode-III loadings, the front may reach different parts of a grain boundary at different times. As the central part of the boundary is exposed to and penetrated through by the front, the grain ahead of the boundary is cleaved. Due to the shielding effect of the crack-tip [18], subsequent cracking behind the verge of propagating front at a different height becomes difficult, especially when the grain boundary toughness is relatively high. Hence, when the next grain is fully separated and the crack front keeps moving forward, the side sections of the grain boundary are left behind, somewhat similar to the bridging reinforcements in a composite material. The nonuniform crack front behavior may also be attributed to the competition of the formation of break-through points along the grain boundary. At the side sections where the confining effect of adjacent grains is pronounced, front penetration can be suppressed, and therefore the front tends to break through the central part of the boundary first, resulting in the irregular boundary failure behavior. This effect can be important if the degree of anisotropy of single crystal is relatively high and the crystallographic orientations of adjacent grains are unfavorable [19].

The fracture work associated with the plastic shearing of a side boundary section can be assessed as [14] $W_1 = k^*\delta_1 w_s \Delta h$, where k^* is the effective shearing strength of grain boundary, which, for the 1010 steel under investigation, can be taken as 120 MPa; δ_1 is the preparatory shearing distance before the abrupt grain boundary separation occurs; w_s is the width of a side boundary section; and Δh is the effective height difference of the two fracture facets across the boundary. The contribution of W_1 to the fracture resistance can be calculated as $G_1 = 2W_1/d_g^2$, where d_g is the grain size. The factor of 2 is used to take into account that there are two side sections at each grain boundary. According to an energy analysis performed by McClintock [20], where the condition of the onset of mode-II fracture following plastic shearing is analyzed based on the data of large-scale punctuation experiment, G_1 should be around 2–5 kJ/m^2, which, while much larger than 2γ (∼0.8 kJ/m^2), is still lower than the measured fracture resistance (∼60 kJ/m^2).

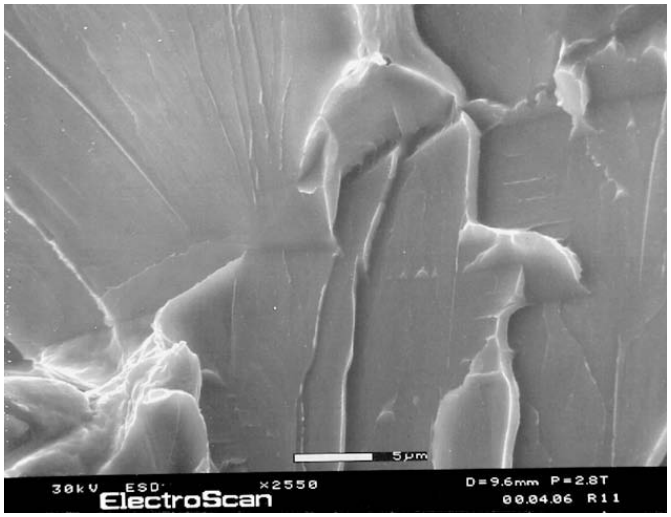

Fig. 2. SEM microscopy of plastic shearing subsequent to cleavage cracking across a high-angle grain boundary. The crack propagates from the bottom to the top.

Before the side boundary sections are separated, the two crack flanks are pinned together locally. As depicted in Fig. 3, assume that initially the crack front is at a regular grain boundary array. It starts to advance from the bottom to the top once the crack growth driving force reaches the critical value, G_{cr}. If a grain boundary is broken through in the regular mode, such as the boundary between grains "A_1" and "B_1", the grain boundary toughness can be assessed by Eq. (1). With the fracture work of lateral grain boundaries, such as the boundary between grains "B_1" and "B_2" being taken into account, the effective local fracture resistance should be calculated by Eq. (2). The boundary between grains "A_2" and "B_2" is dominated by the irregular mode. The crack front can only penetrate through the central part ("bc"), and the side boundary sections ("ab" and "cd") bridge across the fracture surfaces.

With the crack closure, the cleavage front must go a round-about way to bypass the persistent boundary areas, until a new front is formed ahead of the boundary array. If during the front propagation process no external work is input in the system, e.g. in a displacement control experiment, the new front would eventually stop, with an effective crack growth length of Δa. Due to the shielding effect, at a curved crack front [21], the pinning stress at the side boundary sections would cause a negative local stress intensity component at the protruding part of the crack front. Consequently, to keep the front from being arrested, the overall crack growth driving force must be higher than the local fracture resistance. This crack trapping effect is a primary toughening mechanism of composite materials [22,23] and has been investigated intensively for reinforcing fibers and particulates [24–29].

In order to analyze the interruption effect of the grain boundary on the cleavage front behavior, assume that the small-scale yielding (SSY) condition is applicable. Thus [30],

$$P = \delta / C_s \tag{3}$$

where P and δ are the crack opening force and displacement, respectively; and C_s is the effective sample compliance. The strain energy stored in the specimen is

$$U = \delta^2 / 2C_s \tag{4}$$

For a standard double-cantilever beam (DCB) specimen, $1/C_s = Ebh^3/8a_0^3$, with E being the modulus of elasticity, b the specimen thickness, h the height of DCB arm, and a_0 the initial crack length. Before and after the crack front bypasses the boundary, the change in strain energy is

$$\Delta U = \frac{Ebh^3\delta^2}{16}\left[\frac{1}{a_0^3} - \frac{1}{(a_0+\Delta a)^3}\right] + U_2 \tag{5}$$

where U_2 is the strain energy caused by the bridging stress at the side boundary sections. Note that at the onset of crack front advance, the critical energy release rate should be reached, i.e.

$$G_{cr} = -\frac{1}{b}\frac{\partial U}{\partial a}\bigg|_{a=a_0} = \frac{3Eh^3\delta^2}{16a_0^4} \tag{6}$$

The variation in strain energy is balanced by the dissipated work associated with the formation of new fracture surfaces. Thus,

$$\Delta U = (2\gamma)\cdot d_g^2 \tag{7}$$

Substitution of Eqs. (6) and (7) into (5) gives

$$(2\gamma)\cdot d_g^2 = \frac{bG_{cr}}{3}\left[a_0 - \frac{a_0^4}{(a_0+\Delta a)^3}\right] + U_2 \tag{8}$$

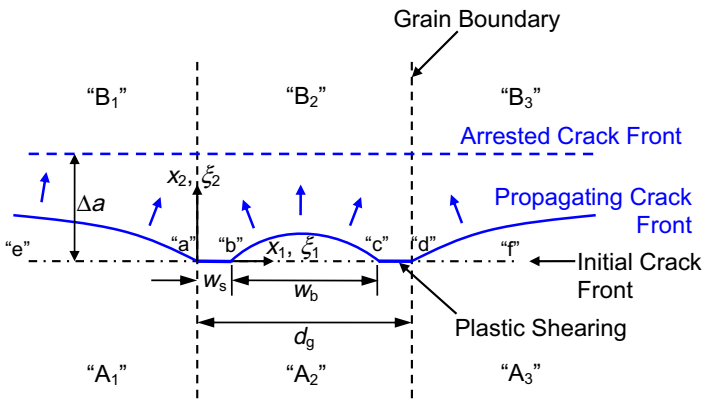

Fig. 3. Schematic of the nonuniform cracking mode.

To calculate U_2, the bridging stress, $\sigma(\xi_1)$, must be obtained, with $\vec{\xi} = (\xi_1, \xi_2)$ being the local coordinate system defined on the side grain boundary section. The subscript "1" indicates the direction parallel to the initial crack front, and "2" indicates the crack growth direction. The range of ξ_1 is $\Gamma = \{(0, w_s) \cup (w_s + w_b, d_g)\}$, where w_b is the width of the central break-through window ("bc") and w_s is the width of side boundary section ("ab" and "cd"). If $\sigma(\xi_1)$ were zero, with the external loading, P, the crack opening distance at the location Δa away from the crack front would be [31]

$$\Lambda_1(\vec{x}) = 2K_1 \frac{1-v}{\mu}\sqrt{\frac{\Delta a}{2\pi}} \tag{9}$$

where v is the Poisson's ratio; μ is the shear modulus; $\vec{x} = (x_1, x_2)$ is the global coordinate system; and K_1 is the average stress intensity factor along the arrested crack front. Since at the steady-state the crack growth step length is much smaller than the total crack length, the dynamic effect on crack-tip stress field is negligible [28]. Under this condition, K_1 can be taken as the average fracture toughness, i.e. $K_1 = \sqrt{EG_1/(1-v^2)}$. With the bridging stress, the local crack closure distance can be calculated as [31]

$$\Lambda_2(\vec{x}) = -\int_\Gamma \left[\frac{1-v}{\mu\rho\pi^2}\arctan\left(\frac{2\sqrt{x_1\xi_1}}{\rho}\right)\right]\cdot\sigma(\xi_1)\mathrm{d}\xi_1 \tag{10}$$

where $\rho = \left|\vec{x} - \vec{\xi}\right|$. The actual crack opening distance should be determined by the grain boundary shearing, which can be described as

$$\Lambda(\vec{x}) = \sigma(\xi_1)/k_{gb} \tag{11}$$

where k_{gb} is the effective shear modulus of the grain boundary. If the shape of the side boundary section is assumed to be triangle and the difference in material properties at grain boundary and inside grain is ignored, k_{gb} can be taken as $E\sqrt{3}$. Combination of Eqs. (9)–(11) leads to

$$\frac{\sigma(\xi_1)}{\sqrt{3}(1-v)} = 2K_1\sqrt{\frac{\Delta a}{2\pi}} - \int_\Gamma \left[\frac{1}{\rho\pi^2}\arctan\left(\frac{2\sqrt{x_1\xi_1}}{\rho}\right)\right]\cdot\sigma(\xi_1)\mathrm{d}\xi_1 \tag{12}$$

Eq. (12) needs to be satisfied for the entire Γ. The additional strain energy associated with the local crack closure can be calculated as

$$U_2 = \frac{1}{2}\int_\Gamma \sigma(\xi_1)\cdot\Lambda(\vec{\xi})\mathrm{d}\xi_1 \tag{13}$$

The bridging stress also affects the distribution of local stress intensity along the arrested cleavage front. In the frame work of linear elasticity, a pair of unit pinning force at ξ would cause a stress intensity factor at s [31]:

$$\widetilde{K}(s) = -\sqrt{\frac{2}{\pi^5}\frac{\sqrt{\Delta a}}{s^2+\Delta a^2}} \tag{14}$$

where s is parallel to ξ_1. Hence, the distribution of stress intensity along the arrested cleavage front is

$$K(s) = \sqrt{\frac{EG_{cr}}{1-v^2}}\left(\frac{a_0}{a_0+\Delta a}\right)^2 - \int_\Gamma \widetilde{K}\cdot\sigma(\xi_1)d\xi_1 \tag{15}$$

The first term at the right-hand side (RHS) of Eq. (15) is the nominal stress intensity factor if the bridging stress did not exist. It can be obtained through Eq. (6) that with a constant crack opening displacement, i.e. without additional input energy, the energy release rate is proportion to $1/a^4$, with a being the crack length. The second term at the RHS of Eq. (15) captures the disturbance caused by the bridging stress. Note that

$$G_1 = \frac{1-v^2}{d_g E}\int_{s=0}^{d_g} K^2(s)ds \tag{16}$$

i.e. the overall crack growth driving force should be balanced by the fracture resistance.

Eqs. (8), (12), (13), and (16) form a complete equation set, through which G_{cr} can be solved. Different from G_1, which is based on the assumption that the crack front propagates uniformly and the central part and the side sections of the grain boundary fail simultaneously, in the calculation of G_{cr} the crack trapping effect of the side boundary sections are taken into consideration. Note that the current analysis is carried out in the framework of linear elastic fracture mechanics (LEFM). Dynamic effects, which may further promote the irregular crack front behaviors, are ignored.

3. Results and discussion

The equation set of (8), (12), (13), and (16) should be solved numerically. In the current investigation, the Ritz method is employed. To solve integral Eq. (12), the bridging stress is taken as

$$\sigma(\xi) = \sum_{i=0}^{4} \alpha_i \xi^i \tag{17}$$

with ξ being the distance to the border of the central part and the side section ("b" and "c" in Fig. 3). It is assumed that the distribution of bridging force is symmetric at the two side boundary sections ("ab" and "cd"), and at $\xi_1 = 0$ and $\xi_1 = d_g$ periodic boundary condition is applied. It was confirmed numerically that including higher order terms in Eq. (17) would only cause negligible changes in the calculation results.

The material parameters, E, v, and μ are used to relate the stress intensity factor, K, to the energy release rate, G. As long as the SSY assumption is valid, K and G should be equivalent to each other [32], and therefore the values of $\{E, v, \mu\}$ do not affect the calculation result of G_{cr}. The numerical results show that when v is in the range of 0.1–0.4 and μ is in the range of 1–1000 GPa, the variation in G_{cr} is less than 5%. The modulus of elasticity, E, also comes in by affecting the nominal crack opening displacement. However, its influence on G_{cr} is still secondary, less than 5% when it varies from 10 GPa to 1000 GPa, probably because that the bridging stress nearly fully closes the local crack flanks. The geometrical factors of the specimen, b, h, and a_0, influence the value of strain energy, but in the calculation of the energy release rate their effects vanish. When they are varied in the range of 1–100 mm, no significant changes in G_{cr} can be detected. Therefore, the model is scalable. As the microstructure at the crack front, which is characterized by w_s, w_b, and d_g, is given, G_{cr} can be obtained as a function of G_1. Note that in a regular grain array w_s, w_b, and d_g are related to each other by $d_g = 2w_s + w_b$. Through a dimensional analysis, their relationship can be described by

$$\widehat{G} = f\left(\frac{w_s}{d_g}\right) \quad \text{or} \quad \widehat{K} = \tilde{f}\left(\frac{w_s}{d_g}\right) \tag{18}$$

where $\widehat{G} = G_{cr}/G_1$, $\widehat{K} = K_{cr}/K_1$, and f and $\tilde{f}$ are two functions to be determined. The critical stress intensity factor, K_{cr}, can be related to G_{cr} by $K_{cr} = \sqrt{EG_{cr}/(1-v^2)}$, and thus $\widehat{K} = \sqrt{\widehat{G}}$.

By substituting Eq. (17) into (12), Eq. (12) can be reduced to a set of algebra equations

$$2\sqrt{3}(1-v)K_1\sqrt{\frac{\Delta a}{2\pi}} - \sum_{i=0}^{4} \alpha_i \bar{\xi}_j^i - \int_{\Gamma} \left[\frac{\sqrt{3}(1-v)}{\rho_i \pi^2} \arctan\left(\frac{2\sqrt{\bar{\xi}_j \xi_1}}{\rho_i}\right)\right] \cdot \left[\sum_{i=0}^{4} \alpha_i \xi^i\right] d\xi_1 = 0 \tag{19}$$

where $\bar{\xi}_j$ $(j = 1, 2 \ldots, 6)$ is the sixth points at the side boundary section (Γ), and ρ_i is the distance between $\bar{\xi}_j$ and $\vec{\xi}$. Thus, Eqs. (8), (13), (16), and (19) can be solved through explicit methods. The ratio of w_s/d_g is varied in the range from 0 to 0.3. In the numerical integration the nearest five grains were considered, and the distributions of bridging stress and local stress intensity are assumed to be periodic, and symmetric with respect to the median plane of the grain.

The results of $\widehat{K}$ (or $\sqrt{\widehat{G}}$) is shown in Fig. 4. By using a polynomial, the numerical data can be regressed as

$$\widehat{K} = \sum_{i=0}^{3} \lambda_i \left(\frac{w_s}{d_g}\right)^i \tag{20}$$

where $\lambda_i = \{1, 18.6, -17.1, 162.9\}$ $(i = 0, 1, 2, 3)$ are coefficients obtained through data fitting. It can be seen clearly that the overall fracture toughness increases rapidly as w_s/d_g becomes larger, as it should, since the larger the portion of the side boundary sections, the more pronounced their crack trapping effect would be. According to the fractography analysis, at a grain boundary that fails in the irregular mode, the two side boundary sections usually take 30–50% of the entire boundary width, and thus w_s/d_g ratio is in the range of 15–25%. From Fig. 4, the value of $\widehat{K}$ is around 4–7; correspondingly, $\widehat{G}$ is around 16–50. Consequently, if only the fracture work of plastic shearing of the side boundary sections is taken into account through

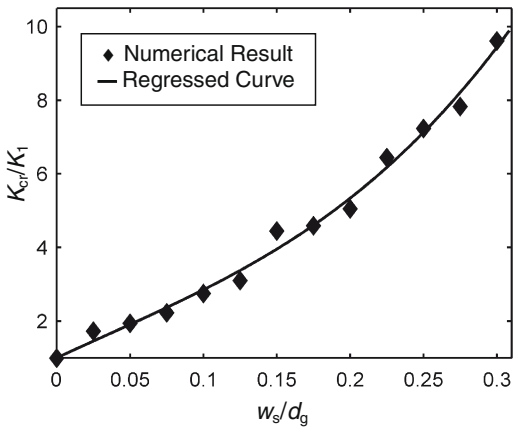

Fig. 4. The fracture resistance as a function of the width of the break-through window.

a simple superposition method, the fracture resistance of the polycrystalline material would be significantly underestimated by more than an order of magnitude. As discussed above, with the fracture work associated with the formation of river markings and the plastic shear of ligaments inside grains being accounted for, the effective surface free energy of a crystallographic plane can be assessed as 0.8 kJ/m^2 [12,33]. By using Eq. (2), the nominal fracture resistance of a polycrystalline material where all the grain boundaries fail in regular mode, G_1 can be estimated as 2.5 kJ/m^2. The actual fracture resistance of the 1010 steel samples under cryogenic condition is 68 kJ/m^2, which is about 27 times higher than the value of G_1, within the predicted range of 16–50. That is, the crack trapping effect of side boundary sections can well explain the large difference between the experimental data and the prediction of Eq. (2).

Fig. 4 indicates that, even when w_s/d_g is only a few percent, the increase in fracture resistance can be large. Compared with the regular-mode fracture resistance (G_1), G_{cr} increases by 40% when w_s/d_g is only 1%; by nearly two times when w_s/d_g is 2%; and by more than an order of magnitude when w_s/d_g reaches 12%. The toughening effect of increasing in w_s/d_g is more pronounced when its value is higher. In fact, theoretically, when w_s/d_g approaches 0.5, the entire boundary becomes unbreakable and the effective fracture resistance tends to infinity. However, under this condition, the weight function method breaks down, and therefore the current study is focused on the range of w_s/d_g ratio from 0 to 0.3.

While the toughening effectiveness of the irregular grain-boundary failure mode is remarkable, it is still not fully understood what are the key factors that trigger such a behavior. From the energy point of view, the most energetically favorable failure mode of a grain boundary in cleavage cracking is the regular mode. On the one hand, as the break-through points are close to each other, the area of grain boundary that needs to be sheared apart is reduced, so that the grain boundary toughness tends to be lower. On the other hand, if the break-through points are too close to each other, the increase in river marking density would cause crack stoppage in the grain ahead of the boundary, even after the boundary is broken through [34,35]. As the two mechanisms compete, the distance between adjacent break-through points varies in a narrow range, leading to the formation of parallel river markings. In the irregular mode, the side boundary sections locally arrest the cleavage front, until both sides of it are cracked. The local crack stoppage should not be attributed to the variation in local fracture toughness, since it is unlikely that at every grain boundary that fails in the irregular mode the toughness is lowest in the central part. It may be related to the profile of the propagating crack front in the grain behind the boundary. With the constraints of the lateral boundary, the central part of the front may protrude and thus reaches and breaks through the boundary first. When the side parts of the front encounters the boundary, the local stress intensity is reduced by the protruding part of the front across the boundary, and therefore the side boundary sections become bridging components. The non-penetration of crack front at side boundary sections may also be caused by the variation in elastic properties across the lateral boundary. For instance, along the direction normal to the median fracture surface, if the adjacent grain is effectively stiffer, the local crack growth driving force near the lateral interface may be lower than that at the central section. Thus, in order to promote the irregular mode, the distribution of crystallographic orientation should be controlled in a certain range. Adjusting the shape of grains may also be helpful. For example, if all the grains are hexagonal, as the crack front propagates along the flat side, it is more likely for the central part of the crack front in each grain to encounter the grain boundary first, compared with the front segments close to the lateral boundaries. If the crack propagates along the sharp angle direction, the side front segments tend to reach the boundary first, and thus regular mode may be dominant.

4. Conclusions

By analyzing the resistance offered to cleavage crack front propagation by side grain-boundary sections, it is found that the toughening effect associated with the irregular boundary failure mode is significant. In such a failure mode, the crack front does not penetrate through the entire grain boundary uniformly. Rather, it first bypasses the boundary in the central part, leaving the side boundary sections behind as bridging components. The side boundary sections are separated apart through plastic shearing, after both sides of them have been exposed to the cleavage fracture surface. The nonuniform crack front behavior causes a significant crack trapping effect, which, in additional to the fracture work of grain boundary separation, can increase the overall fracture resistance by an order of magnitude. A closed-form equation is obtained to capture the toughening effect. Promotion of the nonuniform grain-boundary failure mode may be achieved by controlling the external loading, the texture, and/or the grain shape/size distribution.

Acknowledgement

This work was supported by the Department of Energy under Grant No. DE-FG02-07ER46355.

References

[1] Freund LB. Dynamic fracture mechanics. Cambridge Univ. Press; 1998.
[2] Hertzberg RW. Deformation and fracture mechanics of engineering materials. Wiley; 1995.
[3] McClintock FA, Argon AS. Mechanical behaviors of materials. Addison-Wesley; 1966.
[4] Broberg KB. Cracks and fracture. Academic Press; 1999.
[5] Kovacs I, Zsoldos L. Dislocations and plastic deformation. Elsevier; 1973.
[6] Kelly A, Ashby M, Zweben CH, Baker AA, Beardmore P. Comprehensive composite materials. Pergamon Press; 2000.
[7] Chawla KK. Ceramic matrix composites. Springer; 2003.

[8] Mallick PK. Fiber-reinforced composites. CRC Press; 2007.
[9] Gell M, Smith E. The propagation of cracks through grain boundaries in polycrystalline 3% silicon–iron. Acta Metal 1967;15:253–8.
[10] Gdoutos EE. Fracture mechanics. Springer; 2005.
[11] Hahn GT, Averbach BL, Owen WS, Cohen M. Initiation of cleavage microcracks in polycrystalline ion and steel. In: Proceedings of an international conference on the atomic mechanisms of fracture, Swampscott, MA, April 12–16, 1959. New York: John Wiley & Sons; 1959.
[12] Qiao Y, Argon AS. Cleavage cracking resistance of high angle grain boundaries in Fe–3wt%Si alloy. Mech Mater 2003;35:313–31.
[13] Argon AS, Qiao Y. Resistance of cleavage cracking of high-angle bicrystal grain boundaries in Fe–Si alloy. Phil Mag A 2002;82:3333–48.
[14] Qiao Y, Argon AS. Cleavage crack-growth-resistance of grain boundaries in polycrystalline Fe–2wt%Si alloy: experiments and modeling. Mech Mater 2003;35:129–54.
[15] Qiao Y. The role of recalcitrant grain boundaries in cleavage cracking in polycrystals. J Mater Sci 2005;40:4819–25.
[16] Rao AGM. Fatigue and fracture in steel. Taylor & Francis; 1992.
[17] Qiao Y. Irregular mode cracking in Fe–3wt.%Si alloy. J Mater Sci Technol 2005;21:338–42.
[18] Rice JR. First-order variation in elastic fields due to variation in location of a planar crack front. J Appl Mech 1985;52:571–9.
[19] Kang Y. Experimental analysis for some interfacial mechanics problems. Mech Pract 1999;21:990302.
[20] McClintock FA. A three dimensional model for polycrystalline cleavage and problems in cleavage after extended plastic flow or cracking. In: Chan KS, George R, editors. Irwin symposium on cleavage fracture. TMS; 1997. p. 81–94.
[21] Gao H, Rice JR. A first order perturbation analysis of crack trapping by arrays of obstacles. J Appl Mech 1989;56:828–36.
[22] Bower AF, Ortiz M. A three dimensional analysis of crack trapping and bridging by tough particles. J Mech Phys Solids 1991;39:815–58.
[23] Xu G, Bower AF, Ortiz M. The influence of crack trapping on the toughness of fiber reinforced composites. J Mech Phys Solids 1998;46:1815–33.
[24] Kong X, Qiao Y. Toughening effect of continuous fiber bundles. J Compos Mater 2005;39:1591–602.
[25] Qiao Y, Kong X. Unstable crack advance across a regular array of short fibers in brittle matrix. Compos Sci Technol 2004;64:711–7.
[26] Qiao Y, Kong X. Fracture toughness of thermoset composites reinforced by perfectly bonded impenetrable short fibers. Engng Fract Mech 2004;71:2621–33.
[27] Kong X, Qiao Y. Fracture in ceramic matrix composites reinforced with strongly bonded metal particles. Mech Compos Mater 2005;41:205–16.
[28] Qiao Y, Chakravarthula SS, Kong X. Influence of plastic deformation of particulates on flexure toughness of brittle matrix composite. ASCE J Engng Mech 2005;131:319–23.
[29] Qiao Y. Fracture toughness of composite materials reinforced by debondable particulates. Scripta Mater 2003;49:491–6.
[30] Rice J. Limitations to the small scale yielding approximation for crack tip plasticity. J Mech Phys Solids 1974;22:17–26.
[31] Ulfyand YS. Survey of articles on the application of integral transforms in theory of elasticity. Raleigh (NC): University of North Carolina; 1965.
[32] Anderson TL. Fracture mechanics: fundamentals and applications. CRC Press; 2004.
[33] Qiao Y, Argon AS. Brittle-to-ductile fracture transition in Fe–3wt%Si single crystals by thermal crack arrest. Mech Mater 2003;35:903–12.
[34] Chen J, Qiao Y. Characteristic length scale in cleavage cracking across high-angle grain boundary. Comput Mater Sci 2008;42:664–9.
[35] Chen J, Kong X, Chakravarthula SS, Qiao Y. Grain boundary separation in transgranular cleavage cracking. Mater Res Innov 2008;12:18–23.